Technologies and Materials for Renewable Energy, Environment & Sustainability

Preparation of SnO and SnO_2 Thin Films: Influence of Annealing on Structural, Morphological, and Optical Properties

AIPCP25-CF-TMREES2025-00027 | Article

Preparation of SnO and SnO_2 Thin Films: Influence of Annealing on Structural, Morphological, and Optical Properties

Zinah Abdulateef Abbas[1, a)] Seham Hassan Salman [2, b)]

[1]*Al-Nahrain Research Center for Renewable Energy, AL-Nahrain University, Jadriya, Baghdad 10072, Iraq.*
[2]*Department of Physics, College of Education for Pure Science / Ibn Al-Haitham, University of Baghdad, Baghdad, Iraq.*
[a)]*Corresponding author: zinah.a.a@nahrainuniv.edu.iq*
[b)] *seham.h.s@ihcoedu.uobaghdad.edu.iq*

ABSTRACT. Tin oxide (SnO/SnO_2) thin films with a thickness of about $400 \pm 2nm$ were fabricated on glass substrates using physical vapor deposition (PVD). To assess the effect of thermal treatment, the deposited films were subsequently annealed at 200 °C and 300 °C. X-ray diffraction (XRD) measurements revealed the simultaneous presence of tetragonal SnO and orthorhombic SnO_2 phases in all specimens. After annealing, the diffraction peaks became more intense and narrower, reflecting enhanced crystallinity and grain development. Atomic force microscopy (AFM) showed a marked reduction in root-mean-square (RMS) surface decrease after anealing, accompanied by an increase in mean grain size from (49 – 62) nm. UV–visible spectroscopy indicated high optical transparency (>75%) throughout the visible spectrum. The optical constants (refractive index, absorption index and extinction index) were calculated. The optical band gap chang after annealing.

Keywords: thin films, SnO_2, annealing, physical properties

INTRODUCTION

Tin oxide compounds (SnO, SnO_2, and Sn_3O_4) represent a highly adaptable family of metal-oxide semiconductors distinguished by their adjustable structural, optical, and electronic properties. These materials have attracted considerable attention for use in thin-film transistors, transparent electrodes, gas-detection systems, and a variety of photovoltaic and optoelectronic technologies. Compared with many other wide-bandgap oxides [1][2]. Advances in deposition strategies, post-deposition annealing, and dopant engineering have proven critical in tailoring the microstructure and functional behavior of tin-oxide layers. For instance, UV/O_3-assisted sol–gel methods at low processing temperatures can produce mixed-phase SnO_2 films with enhanced field-effect mobility and improved thin-film transistor characteristics, thus enabling flexible electronic devices [1]. Beyond transistors and solar cells, the sensing performance of SnO_2-based systems has been significantly advanced: La_2O_3/SnO_2 thick films decorated with platinum nanoparticles exhibit heightened CO_2 sensitivity at reduced operating temperatures, emphasizing the impact of surface modification and noble-metal incorporation [3], while Si/SnOx heterostructures reveal how oxygen stoichiometry affects bandgap tuning and current–voltage behavior, a key aspect for future photodetectors and photovoltaic devices [4]. Progress has also been made in optimizing contact and interfacial layers; for example, controlled Gd doping in $AgSnO_2$ contact materials increases both electrical conductivity and mechanical stability [5]. Other reports demonstrate that applying an atomic-layer-deposited Al_2O_3 capping layer to p-channel SnO thin-film transistors reduces oxygen vacancies and boosts hole mobility, leading to improved performance and stability [6]. In parallel, advanced plasma treatments have been shown to refine the electrical properties of n-type SnO_2 thin-film transistors [7]. Against this backdrop, the present research focuses on the fabrication and systematic characterization of SnO and SnO_2 thin films, especially the effect of annealing temperature on their structural, morphological, and optical behavior.

EXPEREMINTAL

Tin oxide thin films with an average thickness of about 400 ± 20 nm were deposited onto pre-cleaned glass substrates by thermal evaporation under high-vacuum conditions. The deposition was carried out at pressures between 2×10^{-5} and 9×10^{-5} bar, with an applied voltage of 60 V and a substrate temperature of 450 °C. A deposition

time of approximately 10 minutes and 56 seconds ensured uniform, well-adherent layers on the glass. Following deposition, the samples were oxidized at 300 °C for one hour while oxygen was continuously introduced until the substrates cooled to room temperature, stabilizing the oxide phase. Post-oxidation annealing was then performed at 200 °C and 300 °C for one hour each to investigate the influence of thermal treatment on the structural and optical characteristics of the films. The crystal structure of the SnO/SnO_2 films was examined using X-ray diffraction (XRD) with Cu-Kα radiation (λ = 1.5406 Å). Scans were taken over the 10°–60° (2θ) range to identify the primary reflections of the SnO and SnO_2 phases. The resulting patterns were analyzed to determine phase composition, degree of crystallinity, crystallite size, and lattice strain using the Scherrer equation. Surface morphology was evaluated by atomic force microscopy (AFM) in tapping mode, providing quantitative measurements of root-mean-square roughness, grain size distribution, and surface uniformity before and after annealing. Optical properties were measured with UV–visible spectroscopy over the 200–1100 nm spectral range. Transmittance data were used to calculate the absorption coefficient, and the optical band gap (Eg) was estimated from Tauc plots by extrapolating the linear region of the $(\alpha h\nu)^2$ versus hν curves to the energy axis. This combined approach of thermal evaporation, controlled oxidation, post-annealing, and multi-technique characterization enabled a thorough assessment of how annealing temperature affects the crystallinity, morphology, and optical behavior of SnO/SnO_2 thin films.

RESULTS AND DISCUSSION

Structural Properties (XRD)

The XRD patterns confirmed the coexistence of tetragonal SnO and orthorhombic SnO_2. In unannealed samples, peaks were broad, indicating poor crystallinity. Upon annealing at 300 °C, sharper peaks corresponding to SnO_2 appeared, signifying improved crystallinity and phase stabilization. Crystallite size also increased with temperature, consistent with grain growth.

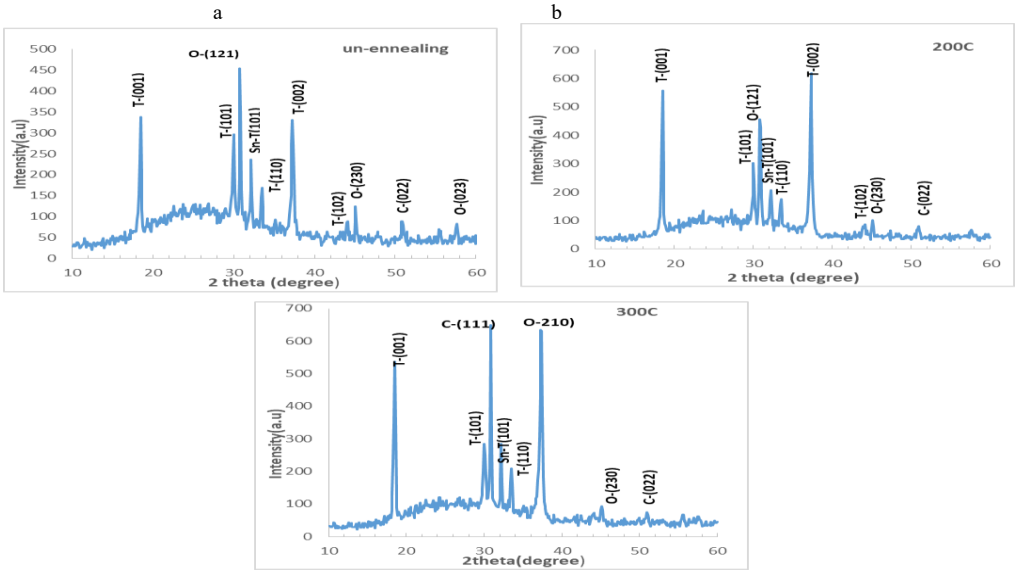

FIGURE 1. XRD pattran of SnOx thin films.

The crystallite size of the thin films was determined by using Scherrer equation [8-11]:

$$Cs = \frac{0.94\lambda}{\beta \cos\theta} \quad (1)$$

The dislocation density (δ), microstrain (ε), and number of crystallites per unit area (N_0) were calculated according to the following relationships [12–18].

$$\delta = \frac{1}{Cs^2} \quad (2)$$

$$\varepsilon = \frac{\beta \cos\theta}{4} \quad (3)$$

$$N_0 = \frac{t}{Cs^3} \quad (4)$$

Where t is the film thickness.

TABLE 1: Standard XRD data of SnO and SnO_2 thin films before and after annealing at 200 °C and 300 °C.

Ta(℃)	cardNo.	phase	$2\Theta_{abs.}$	$2\Theta_{Astand.}$	d_{abs}	d_{astand}	hkl
Un-ennealing	98-018-1280	SnO_2-O	30.847	30.909	2.8962	2.891	121
	00-001-0902	SnO-T	37.31	37.442	2.408	2.400	002
		SnO-T	18.527	18.508	4.785	4.790	001
200	00-001-0902	SnO-T	37.303	37.442	2.408	2.400	002
		SnO-T	18.523	18.508	4.786	4.700	001
	98-018-1280	SnO_2-O	30.857	30.909	2.895	2.890	121
300	98-018-1280	SnO_2-O	30.877	30.909	2.8937	2.890	121
	00-001-0902	SnO-T	37.324	37.442	2.4073	2.400	002
	00-006-0395	SnO-T	18.531	18.508	4.7842	4.700	001

TABLE 2: Crystallite size, lattice strain, and dislocation density values calculated from XRD analysis of SnO/SnO_2 thin films.

Ta ℃	hkl	$2\Theta_{abs.}$	phase	β_{FHWM}deg	C.snm	δ line/m^2*10^{-3}	ε*10^{-3}	N_o
Un-ennealing	121	30.847	SnO_2	0.2623	32.82	0.9284	1.1026	0.0113
200	002	37.302	SnO	0.3498	25.038	1.5951	1.4453	0.0254
300	121	30.877	SnO_2	0.2734	31.489	1.0085	1.1493	0.0128

Surface Morphology (AFM)

AFM analysis revealed that unannealed samples exhibited rough surfaces with RMS roughness of 9.77 nm. After annealing, roughness decreased to 6.33 nm (200 °C) and 5.39 nm (300 °C), while the mean grain diameter increased from ~49 nm (RT) to ~62 nm (300 °C). These changes confirm that annealing promotes smoother, denser, and more uniform films. This dual effect of smoother surfaces and larger grains demonstrates the role of annealing in promoting surface diffusion, densification, and microstructural uniformity.

TABLE 3. Root-mean-square roughness and mean grain size of SnO/SnO_2 thin films as a function of annealing temp.

AnnealingTemp.(℃)	Mean diameter(nm)	Roughness(nm)	Root-mean-square (nm)
R.T	49.15	5.675	9.779
200	67.07	4.829	6.332
300	62.32	4.044	5.393

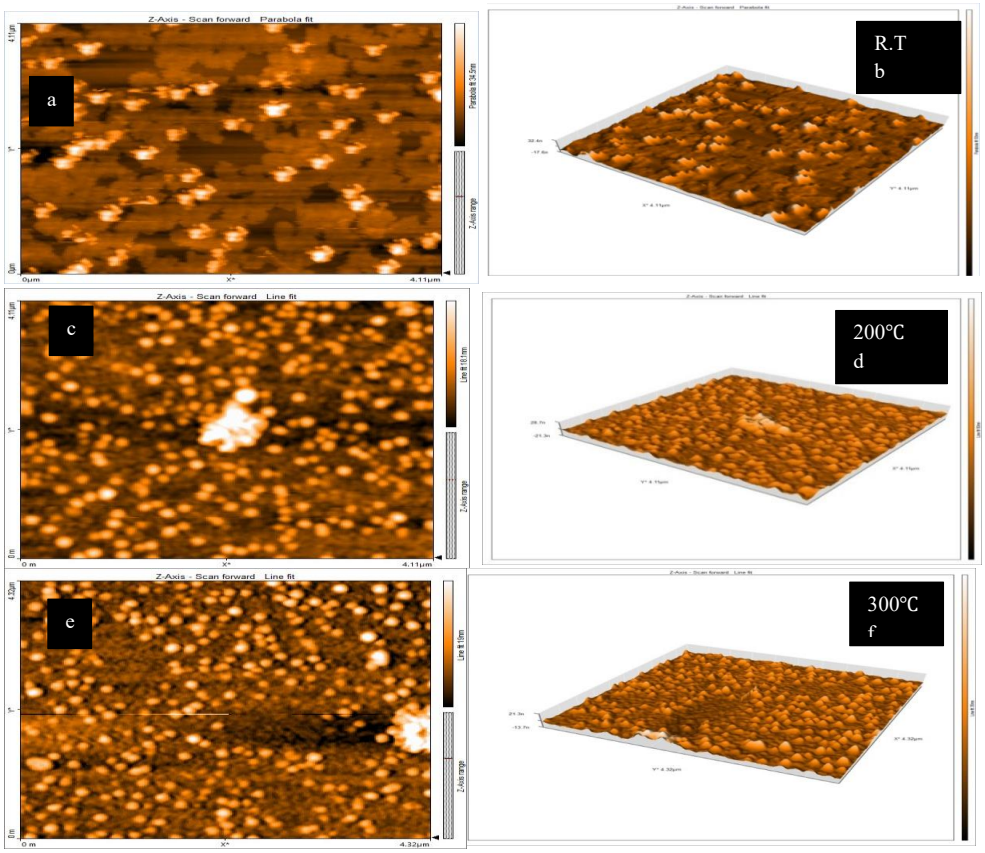

FIGURE 2a,b,c,d,e,f. (AFM) images of SnO/SnO_2 thin films before and after annealing at 200 °C and 300 °C.

Optical Properties (UV-Vis)

UV-Vis spectra revealed high transparency (>75%) across the visible region. The absorption edge shifted towards shorter wavelengths with annealing. Tauc plot analysis showed that the optical band gap increased from 2.8 eV (unannealed) to 2.9 eV after annealing at 200 °C and remained around 2.8 eV after annealing at 300 °C.

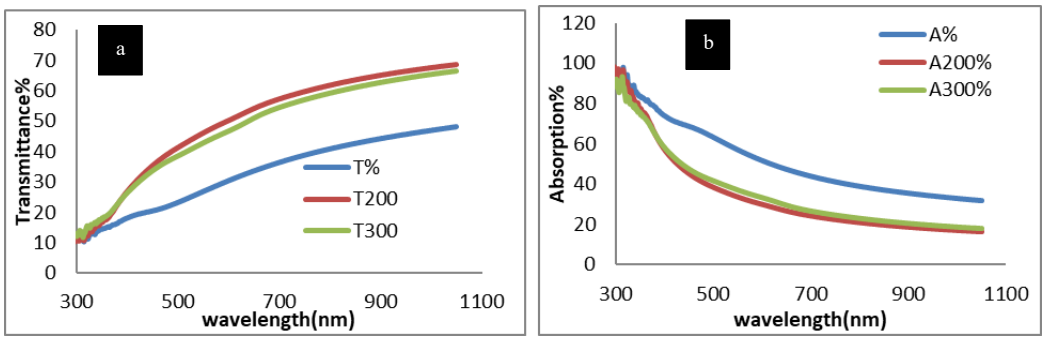

FIGURE 3a,b. Variation of the optical transmittance and absorption spectra of SnO/SnO_2 thin films under different annealing temperatures.

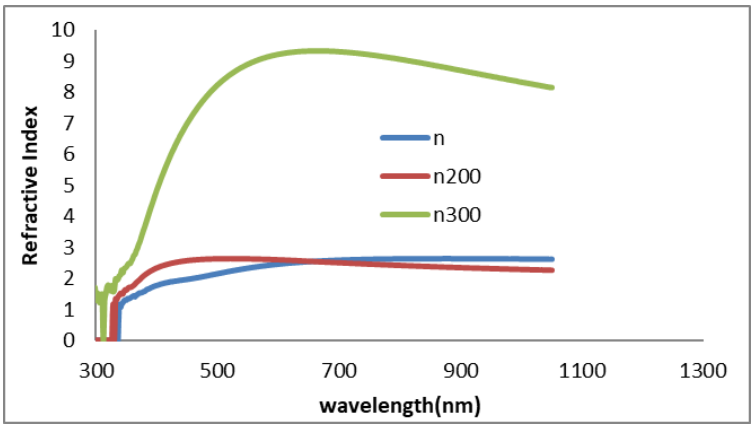

FIGURE 4. Variation of refractive index (n) with wavelength (nm) for thin films.

The refractive index n(an optical constant) is calculated using equation(5) [19].

$$n = \frac{1+\sqrt{R}}{1-\sqrt{R}} \tag{5}$$

Where R is the reflectance, calculated using the equation: [19, 20]

$$R + T + A = 1 \tag{6}$$

Figure 5 shows the change in (α) for tin oxide (SnOx)films which is calculated from relatioshap (5) [19-22]

$$\alpha = \frac{2.303A}{t} \tag{7}$$

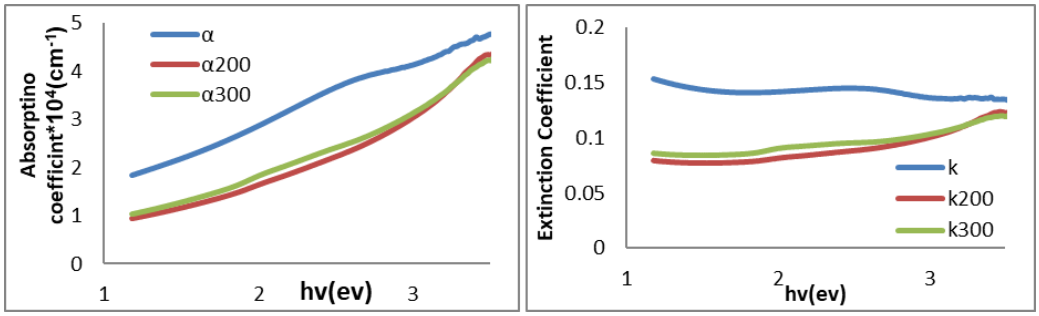

a b

FIGURE 5 a,b. Variation of absorption coefficient (α) and extinction coefficient (k) with photon energy (hv) for thin films.

Figure 5 shows the extinction coefficient (k) for tin oxide films which is calculated from Eq. (8) [19,20].

$$K = \frac{\alpha\lambda}{4\pi} \tag{8}$$

We note from the fig.5 that the extinction coefficient behaves similarly to the absorption coefficient because it depends on the absorption coefficient and the wavelength and depends primarily on the absorption coefficient, and this is consistent with research[20].

Using Tauc's equation (9) [19, 23], the energy gap (Eg.opt) for tin oxide films was calculated.

$$\alpha hv = (hv - Eg)^n \tag{9}$$

where n = 0.5. The linear portion of the $(\alpha h\nu)^2$ versus photon energy ($h\nu$) plot was extrapolated to the $h\nu$ axis, and the point of intersection was taken as the optical band gap. The obtained energy gap ranged from 2.6 to 3.2 eV, as illustrated in Figure 6. These findings are in good agreement with those reported in reference [24].

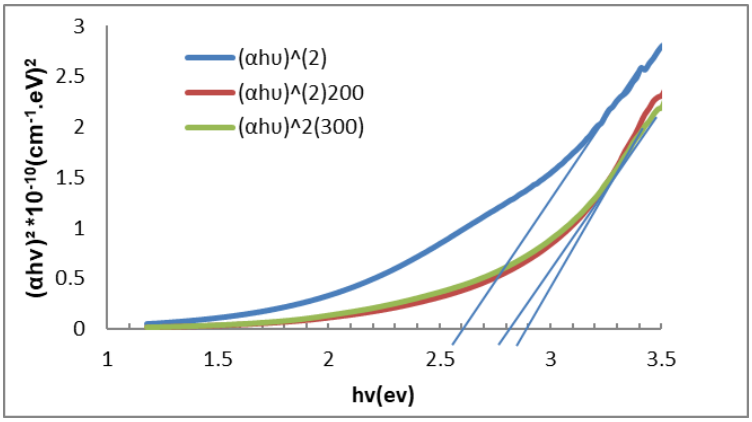

FIGURE 6 . Energy band gap for SnO/SnO_2 thin films.

TABLE 4. Optical factors (Eg.opt, α, n, k,) for of SnO/SnO_2 thin films as a function of annealing temperature.

Temp.ennealing(°C)	A%	α(cm^{-1})	Eg (eV)	n	k
300(R.T)	44.78	3.6378	2.6	2.159	0.144
200	38.35	2.208	2.9	2.6398	0.0878
300	41.51	2.360	2.8	2.6209	0.0951

From table 4 shows optical analysis (UV–Vis) indicates >50% Absorption in the visible region, with a band gap shift from 2.8 to 2.9 eV, stabilizing after higher annealing. This trend suggests that annealing primarily reduces defects and stabilizes the film rather than causing further widening of the band gap beyond 200 °C.

CONCLUSIONS

This study has clearly demonstrated that annealing plays a decisive role in tailoring the physical properties of SnO/SnO_2 thin films. The experimental results confirmed that thermal treatment at 200 °C and 300 °C leads to significant improvements in physical properties of the films. From XRD analysis revealed that the films transitioned from poorly crystalline states in the as-deposited condition to more stable and well-defined phases upon annealing. The diffraction peaks became sharper and more intense with increasing annealing temperature, indicating enhanced crystallinity, grain growth, and phase stabilization. This structural evolution highlights the ability of thermal activation to reduce lattice strain and minimize defect density, both of which are crucial for device-grade films. The surface morphology, studied by AFM, further supported these findings. Unannealed films exhibited high roughness values and relatively small grain sizes, typical of rapid vapor condensation processes. Upon annealing, the RMS roughness decreased markedly from ~9.7 nm to ~6.3 nm (200 °C) and ~5.4 nm (300 °C), while the mean grain diameter increased from ~49 nm to over 62 nm. This dual effect of smoother surfaces and larger grains demonstrates the role of annealing in promoting surface diffusion, densification, and microstructural uniformity. In terms of optical behavior, UV-Vis spectroscopy revealed that the films were highly transparent (>75%) across the visible spectrum, with a slight blue shift in the absorption edge. The optical band gap increased from 2.8 eV (unannealed) to 2.9 eV after annealing at 200 °C, and remained around 2.8 eV after annealing at 300 °C. The improvements in crystallinity, morphology, and optical properties directly translate into enhanced potential for applications in transparent electrodes, optoelectronic devices,

and gas sensors. Moreover, the systematic trends observed at 200 °C and 300 °C provide a clear foundation for future optimization of tin oxide thin films for advanced device applications.

REFERENCES

1. B. Jang et al., "Enhancement Mode Flexible SnO_2 Thin Film Transistors via a UV/Ozone-Assisted Sol-Gel Approach," IEEE Access 8, 123013–123018 (2020). https://doi.org/10.1109/access.2020.3007372
2. N. Ren et al., "25%-Efficiency Flexible Perovskite Solar Cells via Controllable Growth of SnO_2," iEnergy 3(1), 39–45 (2024). https://doi.org/10.23919/ien.2024.0001
3. M. Ehsani, M. N. Hamidon, A. Toudeshki, M. H. Shahrokh Abadi, and S. Rezaeian, "CO_2 Gas Sensing Properties of Screen-Printed La_2O_3/SnO_2 Thick Film," IEEE Sens. J. 16(18), 6839–6845 (2016). https://doi.org/10.1109/jsen.2016.2587779
4. Kumar, M., Srivastava, V. K., Reddy, M. S., Yadav, R. B., Sharma, M., Pal, A., Pandey, P. S., Singh, Y., Singh, G. K., & Singh, B. "Experimental investigation of SI/SnOx Heterojunction for its tunable optoelectronicproperties*", IEEEPhotonicsJournal, 16(5),1*-7(2024) https://doi.org/10.1109/jphot.2024.3452514
5. Y. Zhang, J. Wang, G. Zhang, and Z. Bao, "Research on Simulation, Experiment and Evaluation Method of Different Ratio Gd Doped $AgSnO_2$ Contact Material," IEEE Access 8, 55471–55482 (2020). https://doi.org/10.1109/access.2020.2982015 .
6. K. H. Bae, M. G. Shin, S. H. Hwang, H. S. Jeong, D. H. Kim, and H. I. Kwon, "Electrical Performance and Stability Improvement of p-Channel SnO Thin-Film Transistors Using Atomic-Layer-Deposited Al_2O_3 Capping Layer," IEEE Access 8, 222410–222416 (2020). https://doi.org/10.1109/access.2020.3043780
7. C. Salame, P. Mialhe, and J.-P. Charles, "Effects of the pre-neutron irradiation on VDMOSFET sensitivity to heavy ions," Microelectron. Int. 18, 16–20 (2001).
8. Mohmmad Husain, Seham Hassan Salman," Preparing indium films and studying the effect of oxidation time on their structural and optical properties", Ibn AL-Haitham Journal For Pure and Applied Sciences, 38(2), 156-165. (2025). https://dio.org/10.30526/38.2.4010.
9. S. H. Salman, A. A. Shihab, and A. H. K. Elttayef, "Design and Construction of Nanostructure TiO_2 Thin Film Gas Sensor Prepared by R.F Magnetron Sputtering Technique," Energy Procedia 157, 283–289 (2019). https://doi.org/10.1016/j.egypro.2018.11.192
10. S. H. Salman, N. A. Hassan, and G. S. Ahmed, "Copper Telluride Thin Films for Gas Sensing Applications," Chalcogenide Lett. 19(2), 125–130 (2022). https://doi.org/10.15251/cl.2022.192.125
11. Abdulateef, A.N., Alsudani, A., Chillab, R.K., Jasim, K.A., Shaban, A.H., Calculating the mechanisms of electrical conductivity and energy density of states for Se85Te10Sn5-xInx glasses materials, Journal of Green Engineering, 2020, 10(9), pp. 5487–5503.
12. Hazem, A., & Mustafa, M. H. "Influence of silver doping on the properties of sprayed cadmium Telluride films. *Journal of Physics: Conference Series*, *3028*(1), 012048(2025). https://doi.org/10.1088/1742-6596/3028/1/012048
13. I. A. Abbas and S. H. Salman, "Employment of Titanium Dioxide Thin Film on NO_2 Gas Sensing," J. Phys.: Conf. Ser. 1879, 032061 (2021). https://doi.org/10.1088/1742-6596/1879/3/032061
14. A. H. A. Alrazak, S. H. Salman, I. A. Abbas, M. H. Mustafa, H. M. Ali, and S. A. Abbas, "Influence of Doping with Silver Nanoparticles on the Molybdenum Trioxide Gas Sensor Prepared by Spray Pyrolysis," Dig. J. Nanomater. Biostruct. 20(1), 191–199 (2025). https://doi.org/10.15251/djnb.2025.201.191
15. Shatha F. Abbas, Hiba M. Ali," Improving the properties of NiO films by doping with copper nanoparticles', Journal of Physics: Conference Series 3028 (2025) 012044, https://doi.org/10.1088/1742-6596/3028/1/012044
16. S. H. Salman, S. S. Jahil, N. A. Hassan, S. A. Abbas, and K. A. Jasim, "Ammonia Gas Sensing Using Porous Silicon," J. Phys.: Conf. Ser. 2857, 012051 (2024). https://doi.org/10.1088/1742-6596/2857/1/012051.
17. Hadi, H., Mohammed, K. A., and Hadi, D. "Some physical properties of pure and CU, FE-doped CdS thin films", International Journal of Nanoscience, Vo.. 21(04), (2022). https://doi.org/10.1142/s0219581x22500314
18. S. H. Salman, A. A. Shihab, and A. H. K. Elttayef, "Studying the Effect of the Type of Substrate on the Structural, Morphology and Optical Properties of TiO_2 Thin Films Prepared by RF Magnetron Sputtering," Energy Procedia 157, 199–207 (2019). https://doi.org/10.1016/j.egypro.2018.11.181

19. N.A. Hassan and I.H. Khudayer, “Thickness effect of $CuAlTe_2$ thin films on morphological, structural and visual properties,” Ibn Al-Haitham J. Pure Appl. Sci. 33, 3 (2020). https://doi.org/10.30526/33.3.2471
20. D. Hadi, H. Hadi, and S. H. Salman, “Effect of Annealing on the Physical Characteristics of In_2O_3 Nanoparticle Films,” Ann. Chim. Sci. Mater. 49(3), 315–320 (2025). https://doi.org/10.18280/acsm.490311
21. S. H. Salman, S. M. Ali, and G. S. Ahmed, “Study the Effect of Annealing on Structural and Optical Properties of Indium Selenide (InSe) Thin Films Prepared by Vacuum Thermal Evaporation Technique,” J. Phys.: Conf. Ser. 1879, 032058 (2021). https://doi.org/10.1088/1742-6596/1879/3/032058
22. M. H. Faisal and S. H. Salman, “Effect of Oxidation Times on Gas Sensitivity and Characterization for In_2O_3 Thin Films Produced by Thermal Evaporation,” J. Phys.: Conf. Ser. 2857, 012010 (2024). https://doi.org/10.1088/1742-6596/2857/1/012010
23. N.A. Hassan, Z.N. Jaf, S.H. Salman, I.H. Khudayer, H. Ibrahem and H.A. Miran, “Influence of In-dopant on the optoelectronic properties of thermal evaporated $CuAlTe_2$ films,” Solid State Commun. 371, 115260 (2023). https://doi.org/10.1016/j.ssc.2023.115260
24. H. I. Mohammed, Ghuzlan Sarhan Ahmed, Seham Hassan Salman, Israa Akram Abbas, and Sarah M. Obaid. I-V characteristics of polycrystalline CAZTSe Heterojunction solar cells at different Ag content and annealing temperatures. *International Journal of Nanoelectronics and Materials (IJNeaM)*, *16*(4), 749-758,(2024).. https://doi.org/10.58915/ijneam.v16i3.1341
25. H. S. Wasly, M. S. Abd El-Sadek, S. Elnobi, and A. A. Abuelwafa, “Morphological, Structural, and Optical Properties of Flexible Tin Oxide(II) Thin Film via Thermal Evaporation Technique,” Eur. Phys. J. Plus 137, 164 (2022). https://doi.org/10.1140/epjp/s13360-022-02349-8